Research Square

Preprints are preliminary reports that have not undergone peer review.
They should not be considered conclusive, used to inform clinical practice,
or referenced by the media as validated information.

Consequences of Overtones in Raman Spectra for Structural Assignment of Nickel Anodes during Alkaline Electrolysis

Justus Leist
Institute of Electrochemistry, Ulm University, D-89081 Ulm, Germany
Annika Neufischer
Institute of Electrochemistry, Ulm University, D-89081 Ulm, Germany
Timo Jacob
timo.jacob@uni-ulm.de

Institute of Electrochemistry, Ulm University, D-89081 Ulm, Germany https://orcid.org/0000-0001-7777-2306
Albert K. Engstfeld
albert.engstfeld@uni-ulm.de

Institute of Electrochemistry, Ulm University, D-89081 Ulm, Germany https://orcid.org/0000-0002-9686-3948

Article

Keywords:

Posted Date: December 11th, 2025

DOI: https://doi.org/10.21203/rs.3.rs-8205080/v1

License: This work is licensed under a Creative Commons Attribution 4.0 International License.
Read Full License

Additional Declarations: There is **NO** Competing Interest.

Version of Record: A version of this preprint was published at Nature Catalysis on September 11th, 2026. See the published version at https://doi.org/10.1038/s41929-026-01613-9.

Consequences of Overtones in Raman Spectra for Structural Assignment of Nickel Anodes during Alkaline Electrolysis

Justus Leist, Annika Neufischer, Timo Jacob,* and Albert K. Engstfeld*

Institute of Electrochemistry, Ulm University, D-89081 Ulm, Germany

E-mail: timo.jacob@uni-ulm.de; albert.engstfeld@uni-ulm.de
Phone: +49 (0)731 25401

Abstract

Surface-enhanced Raman spectroscopy (SERS) is a valuable technique, particularly for *in situ* and *operando* studies. However, anharmonic features, such as overtones, while rare and often overlooked, may complicate structural interpretations. This aspect is illustrated for Nickel oxyhydroxide (NiOOH), a vividly discussed oxygen evolution reaction (OER) catalyst for application as anode material in alkaline electrolysers. Based on *in situ* SERS measurements in common electrolytes, including isotope-labeled water and Density Functional Theory (DFT) calculated Raman spectra, we question the presence of NiOOH upon electrochemical oxidation of $Ni(OH)_2$ and instead suggest that the catalytically active surface consists of Nickel dioxide (NiO_2) instead. Additional bands in the experimental spectrum, which were previously assigned to superoxide species, are attributed to overtones and combination bands. Possible reasons for the appearance of overtones are discussed. Previously observed shifts of these bands at varying pH and more positive OER potentials are rationalized by a vibrational Stark effect rather than changes in the material or adsorbate structure.

Introduction

Raman spectroscopy is a versatile technique used for chemical, biological (medical), and material characterization.[1–5] The additional advantage of studying materials immersed in aqueous environments *operando* makes it an indispensable technique for studying catalysts under reaction conditions and gaining atomic scale insights into reaction mechanisms.[6–10] Especially under *operando* conditions, an enhancement of signal intensities is desired, which can be achieved by Plasmon-enhanced Raman spectroscopy (PERS) approaches,[11,12] such as tip-enhanced Raman spectroscopy (TERS),[10] shell-isolated nanoparticle-enhanced Raman spectroscopy (SHINERS),[13] or surface-enhanced Raman spectroscopy (SERS).[1,2,6,8–10] In some cases, the enhancement effect reveals additional bands. These further complicate the already complex interpretation of the spectra and, thus, require additional methods, including density functional theory (DFT) calculations.[2,14,15] Furthermore, in Raman spectroscopy and PERS, only fundamental modes are generally observable, as described by the selection rules in the harmonic approximation.[3,16] However, under certain circumstances the appearance of overtones and combination bands can be observed, such as for molecules,[17,18] graphene,[19–21] MoS_2[22] and WS_2.[23] Considering that overtones are usually not covered (or

even mentioned) in more general reviews on PERS, including recent works on *in situ* and ambient pressure characterization of solid materials,[1,2,6,8,10] raises the question of whether such bands might have been overlooked in some research areas.

In this context, we will illustrate the appearance of such bands in the SER spectra of Ni (oxo-)hydroxides, a widely discussed oxygen evolution reaction (OER) catalyst for application in alkaline electrolyzers.[24–29] Our findings have direct consequences for the interpretation of structural properties, as well as for the ongoing discussions regarding the interpretation of the reaction mechanism, which strongly rely on Raman spectroscopy measurements.[30–34]

Based on the current understanding, it is accepted that under OER conditions, Ni electrodes are oxidized to NiOOH.[35–37] Nevertheless, some puzzles related to the structural properties remain, which, if clarified, will have implications for the description of the reaction mechanism on this surface. For example, the position of the hydrogen atoms is still debated,[38–40] including studies suggesting the presence of delocalized and labile hydrogen atoms.[41,42] Furthermore, it was shown that NiOOH consists of sheets of double hydroxide layers, appearing in two distinct phases (β- and γ-NiOOH). The β-NiOOH phase exhibits a high degree of crystallinity, where Ni is commonly suggested to be in the oxidation state 3.0.[35,36,43,44] In contrast, the disordered γ-NiOOH has been reported to be partially deprotonated and to contain intercalated water or cations, such as K^+.[36,44–46] The oxidation state of Ni in this material has been reported to range between 3.3 and 3.7, suggesting that Ni(IV) is present.[35,43,47–49] Additionally, in recent SERS studies on NiOOH during the OER, an additional band has been reported that could not be attributed to the bulk structure but rather to the formation of superoxides on the NiOOH surface.[32,50,51] In the present work, we will show that the surface likely consists of NiO_2 instead of NiOOH and that the superoxide band is actually related to overtone and combination modes from the NiO_2 spectrum.

To illustrate our reasoning, we first summarize the current understanding of the structural properties of Ni (oxo-) hydroxides before and during the OER, in comparison to experimental *in situ* SER spectroscopy measurements performed in commonly used electrolytes with varying pH, cation species, and isotope composition. Raman spectra inferred from DFT calculations on NiOOH and NiO_2 are used to validate the measured Raman spectra, where the spectrum for NiO_2 (Ni with an oxidation state of 4) best matches the experimental data and accounts for the absence of hydrogen features in the experimental SER spectra. This finding contradicts the prevailing view that the active structure consists of NiOOH. Nevertheless, the experimental Raman spectrum shows additional bands that were previously attributed to superoxide formation, which can only be rationalized by overtone and combination bands from the fundamental modes of NiO_2. Possible reasons for the appearance of these bands are discussed. Furthermore, variations in these bands caused by changing the pH or applied potential might be incorrectly attributed to structural changes or the appearance of intermediates in the reaction mechanism.[32,51] Instead, we illustrate that these changes can be attributed to the vibrational Stark effect. In summary, we show that the assignment of these bands to specific species, rather than overtones, could lead to misinterpretations of the material's structure and reaction mechanisms.

Results and Discussion

Raman Spectroscopy

SERS-active Ni samples were prepared according to the procedure described by Diaz-Morales *et al.*, involving electrodeposition of about 75 layers of Ni on a roughened Au wire.[51] The SERS measurements were performed in a PFA cell designed to minimize the distance the laser has to pass through in the electrolyte, thereby maximizing the resulting signal intensity. Additionally, a stirring rod was included and used during Raman measurements at high overpotentials to disperse bubbles formed during the

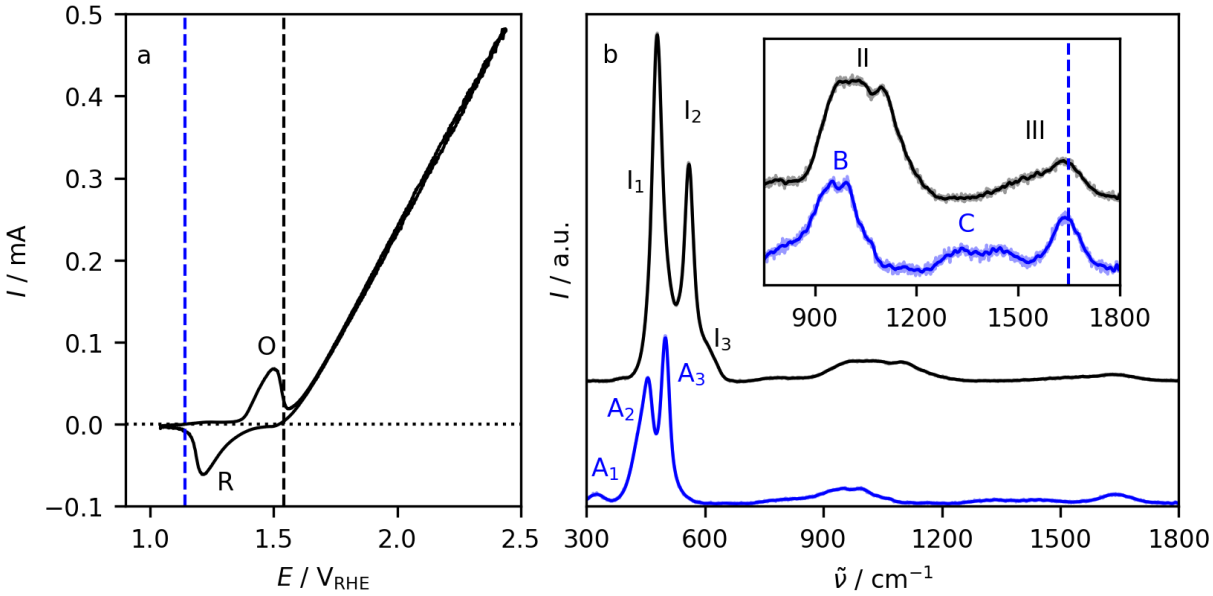


Figure 1: a) Cyclic voltammogram for Au@Ni wire recorded in stirred 0.01 M KOH at a scanrate of 5 mV s^{-1} and limits of 1.04 V and 2.44 V.b) *In situ* SER spectra for Ni in 0.01 M KOH, recorded at electrode potentials of 1.14 V and 1.54 V, at which $Ni(OH)_2$ or NiOOH is formed, respectively. The electrode potentials during both SERS measurements are marked in a. The inset magnifies the region between 800 cm^{-1} and 1800 cm^{-1} by a factor of 10. The labels I_1, I_2 and I_3 refer to the three peaks of the first region at 479 cm^{-1}, 558 cm^{-1} and 610 cm^{-1} of NiOOH whereas II and III refer to the two regions at 900 cm^{-1} to 1200 cm^{-1} and 1400 cm^{-1} to 1800 cm^{-1}. Furthermore, the position of the H_2O bending vibration is highlighted in blue for both $Ni(OH)_2$ and NiOOH.

OER and thereby reduce noise. Details on the sample preparation, the electrochemical cell, procedures, as well as the background and noise correction applied to all SER spectra are provided in the SI.

A cyclic voltammogram for the SERS sample recorded in stirred 0.01 M KOH at a scan rate of 5 mV s^{-1} is shown in Fig. 1a, featuring typical redox features for Ni electrodes in this potential region.[26,36,37,52,53] According to previous reports, in the positive-going scan $Ni(OH)_2$ is oxidized to NiOOH in the oxidation peak O, with a maximum of 1.49 V. The reverse reaction occurs in the reduction peak R with a maximum of 1.2 V in the negative-going scan.[32,51,54,55]

The change in the structural properties during the oxidation in peak O is apparent from *in situ* SER spectra in Fig. 1b, recorded at electrode potentials of 1.14 V (blue) and 1.54 V (black) (also marked in Fig. 1a by vertical lines). Further SER spectra recorded in steps of 0.1 V between these limits are included in the SI (Fig. S5).

The SER spectrum for $Ni(OH)_2$ is similar to those reported previously, containing in region A three distinct peaks at 324 cm^{-1} (peak A_1), 454 cm^{-1} (peak A_2) and 499 cm^{-1} (peak A_3).[32,42,51,56–58] The modes at 454 and 499 cm^{-1} were assigned to E_g or A_{1g} representations of the corresponding point group D_{3d}, while the mode at 324 cm^{-1} was assigned the E_g irreducible representation.[42] Additional bands appear between 850 cm^{-1} and 1100 cm^{-1} (region B) and 1200 cm^{-1} to 1500 cm^{-1} (region C). Region B has been observed both *in situ* and under ambient conditions (and high pressure).[32,59] In the latter case, the band was assigned to an E_g mode.[59] Region C has, to the best of our knowledge, not been reported before. Finally, the feature at 1650 cm^{-1} corresponds to the bending vibration of water.[60]

When the electrode potential is increased to 1.54 V, the SER spectrum changes significantly, as reported in numerous previous

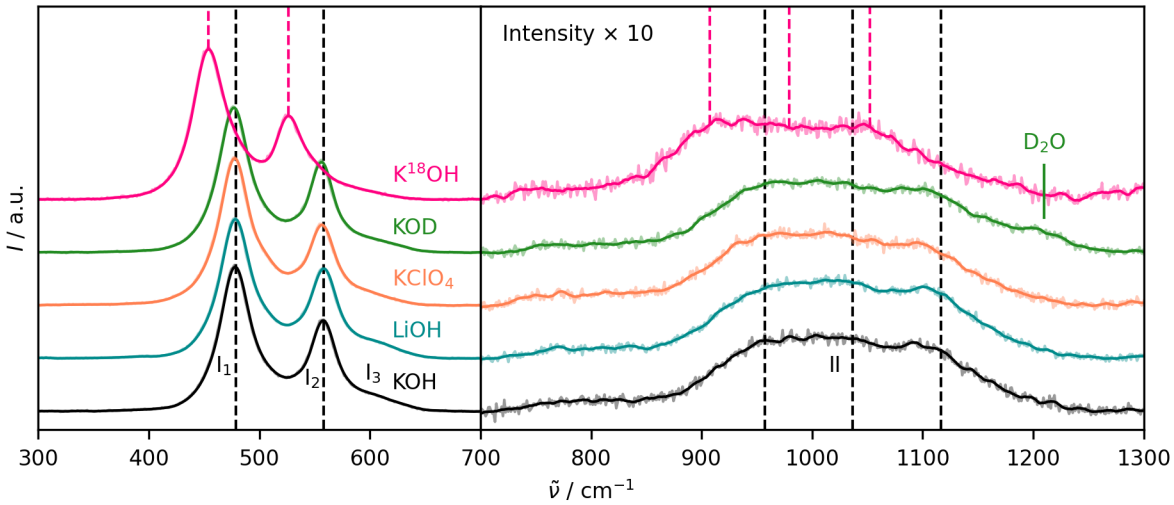


Figure 2: *In situ* SER spectra of NiOOH in 0.01 M KOH, LiOH, $KClO_4$ (pH=8.5), KOD and $K^{18}OH$ with an applied potential of 1.54 V without stirring. The intensity scale is increased by a factor of 10 after 700 cm^{-1}. The four main features of NiOOH at 479, 560, 610 and 900-1200 cm^{-1} measured in 0.01 M KOH are labeled as I_1, I_2, I_3 and II. Features I_1 and I_2 measured in KOH are marked in black dashed lines. Conversely, features I_1 and I_2 measured in $K^{18}OH$ are marked with magenta dashed lines. Overtones for KOH (black) and $K^{18}OH$ (magenta) are calculated using features I_1 and I_2 from KOH and added to region II. Measurements in KOD include the D_2O bending vibrations at 1210 cm^{-1}.

studies.[32,42,50,51,54,55,61–70] Possible changes at higher potentials will be discussed further below. In region I, the peaks A_1 to A_3 assigned to $Ni(OH)_2$ before the oxidation peak O disappear upon increasing the potential, and two intense modes at 479 and 558 cm^{-1} denoted as I_1 and I_2 emerge. Studies aiming at assigning these peaks are scarce. Mostly, these are related to Ni−O or Ni−OH moieties of NiOOH.[51,54,70] Similar peaks have been observed for both β- or γ−NiOOH,[32,55,69] hence, following, we simply refer to NiOOH.

A shoulder at 610 cm^{-1} (peak I_3) has been observed previously, but an explanation of its origin is still missing.[32,50,51,54,55,61–68] Additional bands appear at wavenumbers larger than 700 cm^{-1}, which we separate into two regions, *i.e.*, region II from 900 cm^{-1} to 1200 cm^{-1} and region III from 1400 cm^{-1} to 1800 cm^{-1}.

Region II has been vividly discussed previously, especially with respect to possible reaction intermediates during alkaline OER.[32,33,50,51,67,68] It was concluded that the region consists of several convoluted peaks, which are possibly related to Ni superoxides (Ni−OO^-),[32,50,51,71] discussed in more detail below. Finally, region III from 1400 cm^{-1} to 1800 cm^{-1} has not been observed previously. The peak at 1650 cm^{-1} corresponds to the water bending vibration,[60] which can be substantiated by additional measurements in KOD (see Fig. S8 in the SI).

Ambiguous assignment of Raman peaks in the literature can be caused by the fact that SERS measurements carried out by different groups are generally conducted under dissimilar experimental conditions, such as sample preparation, choice and structure of the SERS substrate, electrolytes used, and the employed excitation laser (wavelength and power). To mitigate related issues and to summarize recent results, we recorded *in situ* SER spectra for Au@Ni electrodes at 1.54 V in different commonly used electrolytes, shown in Fig. 2. Specifically, measurements were performed using 0.01 M KOH (black), LiOH (light blue), $KClO_4$ (orange), KOD (green), and $K^{18}OH$ (pink), where re-

gion I and region II are highlighted in Fig. 2a and b.

The peaks in region I and II are almost identical, upon changing the electrolyte from KOH to LiOH, indicating that these peaks do not depend on the cation type. A similar observation has been reported previously, where SER spectra recorded in KOH were compared to those recorded in CsOH.[32] Using a range of alkali metal ions (Li, Na, K, and Cs), other authors report that depending on the alkali metal ion used, the features change in region I[27] and region II.[64] Some authors suggest that the features in region II are related to superoxides (discussed below), and hence, the changes in region II were rationalized by the interactions of the alkali metal ions with these superoxides.[64]

Using $KClO_4$ (pH =8.5, orange spectrum) did not reveal any measurable changes in either region I or II compared to measurements performed in KOH (black) and LiOH (blue). This result suggests that, in contrast to previous reports, our results indicate that the pH has no effect on the underlying structures.[51,70] Adsorbed ClO_4^- is commonly observed at 930 to 950 cm^{-1} but is not measurably observed in our SER spectrum.[72]

The possible presence of hydrogen atoms in the NiOOH structure is elucidated through measurements using isotope-labeled water. The SER spectrum recorded in KOD (black) compared with that recorded in KOH (green) does not reveal any measurable changes, except for a small shoulder at around 1210 cm^{-1} in KOD, which can be attributed to the D_2O bending vibration.[60] Similar results have been reported previously,,[32] suggesting that hydrogen is absent.[69] The absence of H in NiOOH has also been indicated by UV-vis reflectance spectroscopy studies.[73] On the other hand, previous work using infrared spectroscopy and inelastic neutron scattering revealed the formation of hydrogen-bonded hydroxyl groups in the bulk structure, and further suggested that protons are delocalized.[41,42,74,75] Thus, the behavior of protons in NiOOH is not yet fully understood.

Using labeled oxygen ($K^{18}OH$), the peaks I_1, I_2 and I_3 shift from 479, 559 and 610 cm^{-1} to lower wavenumbers, *i.e.*, 462, 534, and about 590 cm^{-1}. Also, region II shifts to lower wavenumbers compared to measurements in KOH, as reported previously.[32,51]

In total, based on the shifts observed in $K^{18}OH$ in region II and the suggested lack of hydrogen species (inferred from measurements in KOD), region II is commonly associated with peroxide or superoxide species, which have been discussed as active oxygen species during the OER.[32,50,51,70,71] However, since region II appears already before the onset of the OER, some authors argued that bands in this region must be related to lattice moiety instead of an active oxygen intermediate.[32] Moreover, region II consists of a rather broad band, which is somewhat unexpected for superoxides, which, for other systems, such as CeO_2 and Pt oxides, usually consist of fewer and sharper peaks.[76,77] Consequently, the precise origin of region II remains unclear.

Density Functional Theory

The peaks I_1, I_2, and I_3 in the experimental SER spectra of NiOOH have not yet been unambiguously assigned to a specific surface structure. Nevertheless, a significant number of theoretical studies report on various properties of NiOOH, predominantly focusing on the structure of NiOOH at the onset or during the OER.[38,78–84] However, none of the theoretical studies explicitly show computed Raman spectra and, hence, a direct correlation between experiment and theory is not met.

To approach this issue, we computed SER spectra for various bulk and surface structures with periodic DFT calculations using the Vienna *ab initio* Simulation Package (VASP) utilizing the PBE exchange-correlation functional and the Projector augmented wave (PAW) method.[85–88] Additionally, DFT-D3 corrections were employed to account for dispersion interactions.[89] Detailed information on the calculations, considered structures, and the calculated Raman spectra can be found in Section S9 in the SI.

To interpret the experimentally measured SER spectra, we considered four structures in our computational study, *i.e.*, NiOOH and

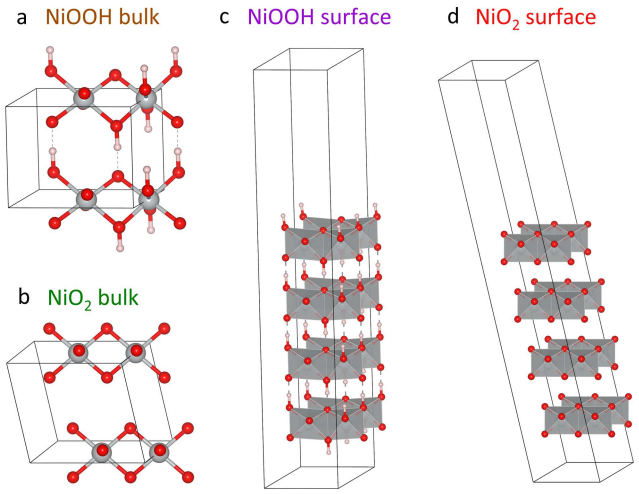


Figure 3: Relaxed structures of NiOOH bulk, NiO_2 bulk, NiOOH and NiO_2 surface slabs used for the DFT calculations and the resulting Raman spectra in Fig. 4.

NiO_2 bulk systems as well as a (0001) surface for each of these Ni-oxides, see Fig. 3. Based on previous studies,[38,43] we adopted a Brucite-type structure for bulk β-NiOOH (Fig. 3a), which is similar to that of $Ni(OH)_2$ with half of the hydrogen atoms removed). We further consider an ABBCCA O-layer stacking order as suggested by theory.[38] For the bulk NiO_2 structure, the H atoms of bulk β-NiOOH were removed, and the structure was relaxed. As a result, the ABBCCA O-layer stacking order transformed into an ABAB stacking order. Finally, for both NiOOH and NiO_2, a structure was calculated with 15.1 Å or 14.4 Å of vacuum above the surface. The corresponding calculated Raman spectra for all structures are shown in Fig. 4, including the experimental data for reference. Full spectra for both NiOOH structures with additional modes below 300 and above 1300 cm^{-1} are shown in Fig. S9 in the SI, along with tables listing the position of each mode for all structures.

We first focus on the computed Raman spectra of the NiOOH structures in Fig. 4a. For the bulk structure of β-NiOOH, three modes are observed below 600 cm^{-1}. The two peaks at 458 and 576 cm^{-1} are close to the peaks I_1 and I_2 found in the experiment, but the intensity ratio is opposite. The mode with the highest

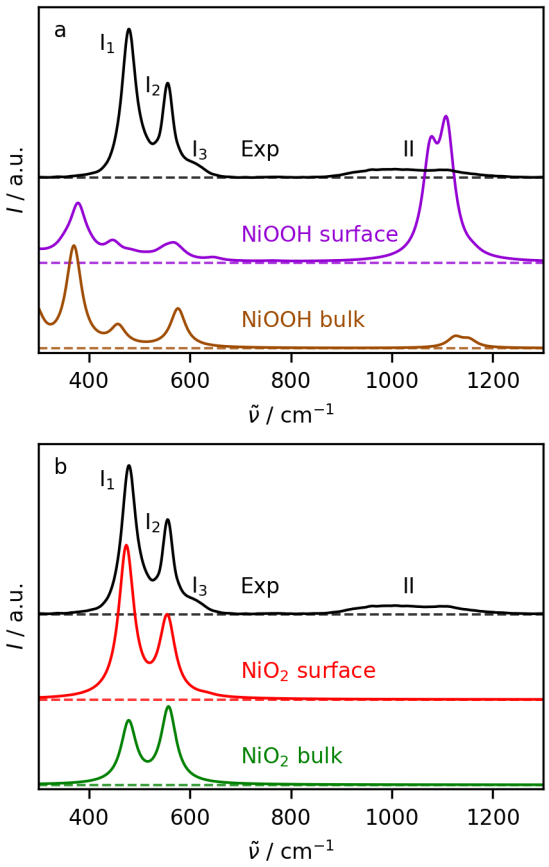


Figure 4: (a): Raman spectra of of NiOOH bulk and NiOOH surface (b): Raman spectra of NiO_2 bulk and NiO_2 surface. Calculated spectra are displayed using an arbitrary Lorentzian peak width for comparison with experimental data. Experimental SER spectra in 0.01 M KOH at 1.54 V measured without stirring added to (a) and (b).

intensity at 370 cm^{-1} is, however, missing in the experimental spectrum. A further broad band is predicted between 1125 cm^{-1} to 1153 cm^{-1} which overlaps with region II in the experimental spectrum. According to the computational model, the band corresponds to an OH bending vibration. The peak I_3 observed in the experiment is not present in the computed spectrum. Further peaks are predicted at 294 cm^{-1} and 2234 cm^{-1} (see Fig. S9 in SI), of which the latter corresponds to an OH stretching vibration. Neither of these peaks are observed in the experimental spectrum.

The computed spectrum of the NiOOH surface (brown) is similar to that of the NiOOH

bulk (purple). The peaks of the surface at 256 cm^{-1}, 379 cm^{-1}, 445 cm^{-1}, 541 cm^{-1} and 647 cm^{-1} are prominent, with the peak at 379 cm^{-1} having the highest intensity. Furthermore, the O−H bending band from 1076 cm^{-1} to 1109 cm^{-1} appears with relatively high intensity. Finally, the O−H stretching vibration is predicted by intense peaks at 2273 cm^{-1} and 3730 cm^{-1} (Fig. S9). Similar to the calculated Raman spectrum for the bulk structure, only peaks at 445 cm^{-1} and 541 cm^{-1} can be vaguely attributed to I_1 and I_2, while the other predicted peaks are not present in the experimental spectrum. As not all predicted peaks appear in the experimental spectrum of NiOOH and as the isotope-labeled SERS measurements indicate a lack of hydroxyl groups, we suggest that the near-surface region in the experiment accessible by Raman spectroscopy does not contain any OH species.

A potential hydrogen-free structure is NiO_2, whose structure is based on deprotonated NiOOH. The corresponding computed Raman spectra for a NiO_2 bulk (green) and surface (red) are shown in Fig. 4b, including the experimental Raman spectrum (black). The Raman spectrum for the NiO_2 surface (green) shows two peaks at 479 and 558 cm^{-1}, which almost perfectly match the position of the peaks I_1 and I_2 in the experimental spectrum. However, the peak intensities differ, where the peak at 558 cm^{-1} has a higher intensity than the peak at 479 cm^{-1} compared to the experimental spectrum. The peaks can be assigned the symmetries E_g and A_{1g}, considering that the NiO_2 structure belongs to the point group D_{3d}. Two additional modes are predicted at 548-551 and 627 cm^{-1}, corresponding to the symmetry A_{2u} and E_u modes, that can also be rationalized by group theory. However, due to their symmetry properties, they are not Raman active, and thus are not attributed a relevant intensity by the DFT calculation. Peak I_3 and peaks in the region between 900 and 1200 cm^{-1} are not present in the computed spectrum. No further peaks are observed beyond the region shown in Fig.4.

The calculated Raman spectrum for the NiO_2 surface (red) in Fig. 4b shows two bands at 474 and 557 cm^{-1} which match the position of peaks I_1 and I_2 in the experiment. In this case, the predicted intensities resemble more closely that in the experimental spectrum. Both peaks can again be assigned the symmetry E_g and A_{1g}. Additionally, the calculation of the surface predicts two additional, less intense modes at 552 (which is concealed by the A_{1g} mode) and 634 cm^{-1} (visible as a small shoulder upon close inspection). These modes correspond to E_u and A_{2u} symmetries of the NiO_2 bulk structure and are usually not expected to be Raman active. Nevertheless, DFT calculations predict small Raman activities for both modes. The appearance of these modes can be explained by a distortion of the symmetry at the surface of a NiOOH surface, which disrupts the symmetry of the E_u and A_{2u} modes. Therefore, the selection rules are lifted, allowing both modes to become Raman active.[90–95] The A_{2u} mode of NiO_2 surface at 634 cm^{-1} appears at a similar position as peak I_3 of the experimental Raman spectrum, suggesting that both peaks are related.

In total, the SER spectrum of NiOOH measured at 1.54 V in 0.01 M KOH (black curve) can be accurately described by the DFT calculation using a NiO_2 surface (red curve). This comparative experimental and theoretical study further substantiates the claim that the NiOOH surface is deprotonated. In addition, given that the here calculated NiO_2 structure contains Ni in an oxidation state of IV, the formation of such oxidation states on the surface of NiOOH warrants further discussion, which will be addressed further below.

Overtone and combination modes

An often overlooked aspect in the interpretation of Raman spectra is the role of overtones, also referred to as higher-order harmonics or higher-order scattering. In general, overtone and combination modes in Raman spectra would be forbidden according to the selection rules in the harmonic approximation. However, as described in the introduction (and below), under certain conditions, such features can appear.[3,16] Within the harmonic approximation, the posi-

tions of overtones correspond to integer multiples of fundamental modes, while combination modes result from sums of different fundamentals.

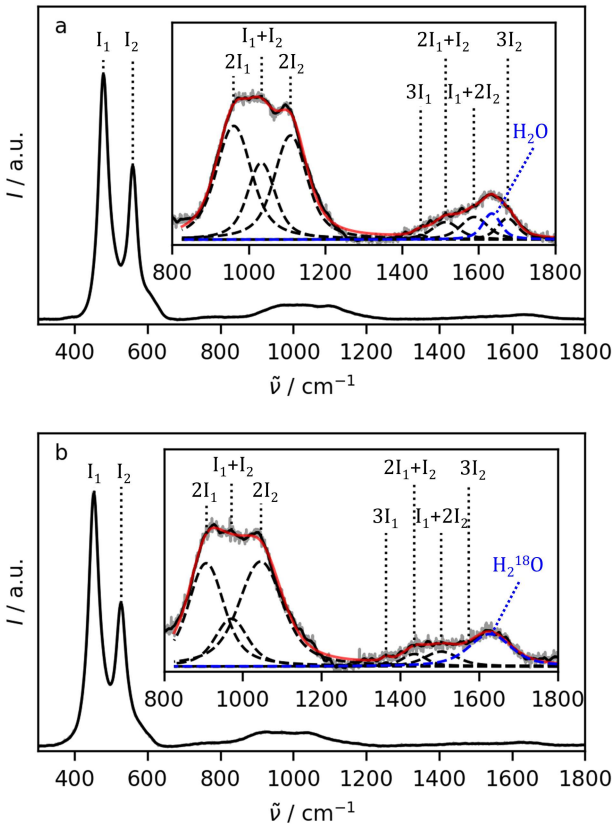


Figure 5: a) *In situ* SER spectra of NiOOH in 0.01 M KOH with an applied potential of 1.54 V up to 1800 cm^{-1}. b) *In situ* SER spectra of NiOOH in 0.01 M $H_2{}^{18}O$ with an applied potential of 1.54 V up to 1800 cm^{-1}. The inset of both spectra highlights the first and second overtone and combination bands. The position of possible overtone, combination modes, and the position of the $\nu_2(H_2O)$ bending vibration of water are highlighted. Using only the calculated position within a margin of ± 10 cm^{-1} of the predicted peaks, the spectra in the inset were deconvoluted. Additionally, the deconvolution contained H_2O or $H_2^{18}O$ bending vibration.

To discuss the role of overtones, we highlight region II and III of the experimentally measured SER spectrum of NiOOH (NiO_2 based on the DFT results above) in the inset of Fig. 5a and indicate possible overtone and combination modes. The first overtones for the peaks I_1 and I_2 are expected at the positions $2I_1$ and $2I_2$, and the combination of both modes would appear at the position $I_1 + I_2$ (marked in the inset). These peaks are all within region II of the SER spectrum. Using the positions of these overtones and the combination band, we deconvoluted region II into three peaks (dashed curves in the inset of region II), where the sum of the peaks (red curve) follows the experimental Raman spectrum in this region. Details on the fitting procedure are provided in Section S4 in the SI. The positions of the most relevant deconvoluted peaks for the discussion are summarized in Table 1, including overtones in KOD (Fig. S8) and $K^{18}OH$ (Fig. 5b).

Elaborating further on possible higher overtones, we suggest that region III (1400 cm^{-1} to 1800 cm^{-1}) consists of the second overtones of the fundamental peaks I_1 and I_2, as well as the combination modes from these peaks. To deconvolute this region, we also considered the band related to the bending mode of H_2O (marked in blue). In addition, combination bands with peak I_3 are expected to appear within the respective overtone regions. However, the intensity is presumably too low to provide a significant contribution to the measured signal in this region. A similar approach can be used for SER spectra recorded in KOD, where in addition, the bending vibration related to D_2O at 1200 cm^{-1} has to be taken into account, as demonstrated in Fig. S8 in the SI.

More interesting is the deconvoluted SER spectrum for NiOOH recorded in $K^{18}OH$, shown in Fig. 5b. Here, the fundamental modes (peaks I_1 and I_2) shift to lower wavenumbers. Hence, the overtones and combination modes also shift to lower wavenumbers in regions II and III. The peak related to $H_2{}^{18}O$ at 1618 cm^{-1} is considered in the deconvoluted SER spectrum. Consequently, previous studies claiming that this region is associated with oxygen are, in principle, true. But the shift of region II and III is only an indirect effect, caused by the shift of the fundamental modes, and is likely not related to possible oxygen species (superoxides) present on the electrode surface at these potentials. In

Table 1: Position of the fundamental modes (from the experimental SER spectrum), and position of the deconvoluted overtone, and combination modes (given in cm^{-1}) of the Raman spectrum in Fig. 5 and Fig. S8 in SI. Peak I3 is marked with a * since the exact position of its maximum can not be determined. Since the intensity of peak I3 is low, overtone and combination modes with this peaks were not considered for deconvoluting the spectra in Fig. 5. The estimated positions of these modes are listed and likewise marked by a *.

	Region	KOH	KOD	$K^{18}OH$
I_1	I	479	481	454
I_2	I	560	560	528
I_3*	I	610*	610*	590*
$2I_1$	II	961	966	908
$I_1 + I_2$	II	1033	1042	972
$2I_2$	II	1109	1115	1046
$I_1 + I_3$*	II	1090*	1090*	1044*
$I_2 + I_3$*	II	1170*	1170*	1118*
$2I_3$*	II	1220*	1220*	1180*
$3I_1$	III	1449	1452	1364
$2I_1 + I_2$	III	1514	1511	1436
$I_1 + 2I_2$	III	1589	1591	1504
$I_1 + 2I_2$	III	1676	1669	1574
H_2O	III	1634	1195	1628

total, the appearance of overtones would also explain why region II is not reproduced by the DFT calculation. These modes arise from anharmonic effects, which are not accounted for by the finite difference approach that we employed to calculate phonon modes.

Interestingly, overtones are also apparent in the *in situ* Raman spectra of oxidized Ni sheets without SER support, measured under similar conditions, albeit with reduced intensity as demonstrated in Fig. S5 in the SI. Therefore, it is unlikely that the observed overtones originate from a SERS effect. In contrast, a Raman spectrum for $Ni(OH)_2$ can only be observed, in the presence of a SER substrate (blue curve in Fig. 1b). Here, the additional features B and C in the experimentally obtained SER spectrum can also be explained by overtones, as demonstrated in Fig. S7 in the SI.

Following, we briefly discuss possible reasons for the appearance of overtones. The most common explanation would be a relation to the resonance-enhancement effect, which was previously proposed for NiOOH for excitation at a laser wavelength of 633 nm.[51,63] In contrast, no resonance effect is known or stands out for $Ni(OH)_2$ at this wavelength. While first overtones can occur due to resonance Raman scattering in form of triple Raman scattering resonance, the occurrence of a complete second overtone band is unlikely.[3,16,20,22,96] Hence, resonance enhancement alone does not fully rationalize the observed overtone features in our case. Considering reports on overtones and combination modes for other systems, it seems these features appear predominantly in layered materials such as MoS_2,[22] WS_2,[23] graphene oxide,[97] transition metal oxides such as $LiCoO_2$ (under ambient conditions and *in situ* dissolved in propylene carbonate),[98] or RuO_2.[99,100] For some of these systems, overtone and combination modes were also suggested to be related to resonance effects.[22,23,97] In general, layered materials are prone to defects and mismatches due to comparably weak interlayer interactions.[101,102] Therefore, we suggest that the overtones exhibited by these materials might be enhanced or even induced by such defects generated by the intermolecular interactions between the layers. Further detailed studies are, however, required to substantiate this assumption.

Vibrational Stark effect

So far, our results and discussion were based on the Ni oxide structure found at around the onset of the OER. Following, we illustrate the consequences of addressing the peak in region II to overtones on the interpretation of SER spectra recorded during the OER, i.e., at higher overpotentials. where this feature is usually attributed to superoxides.[32,51] Therefore, we performed *in situ* SERS measurements on the Au@Ni electrodes in 0.01 M KOH at potentials between 1.54 to 2.74 V Fig. 6a. Furthermore, to elucidate possible pH effects in this potential region, we show in Fig. 6b, SER spectra recorded in 0.1, 0.01 and 0.001 M KOH.

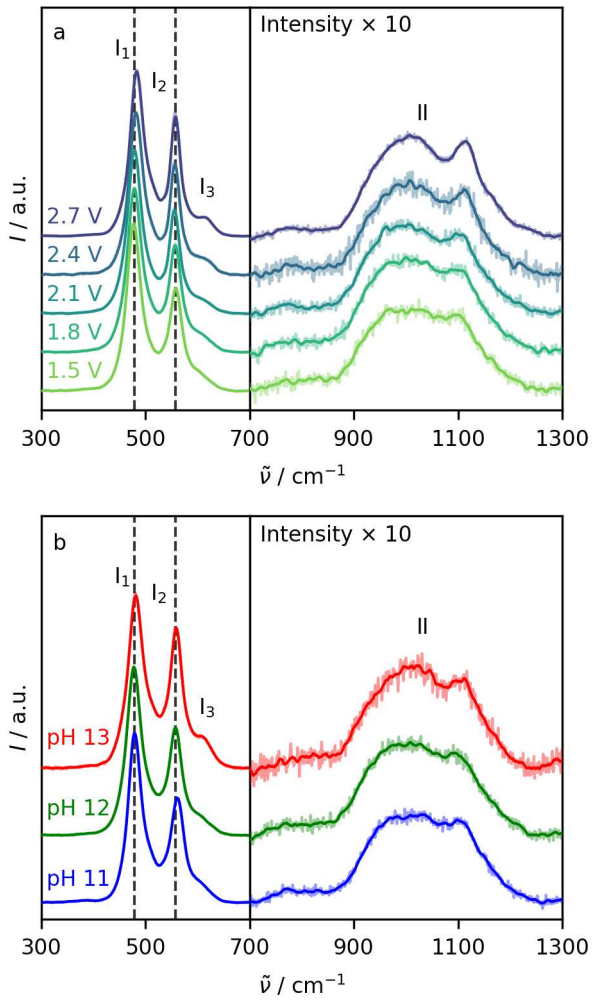


Figure 6: a) SER spectra of Ni from 1.54 to 2.74 V recorded in 0.01 M KOH. b) SER spectra recorded at 1.64 V in 0.1 M, 0.01 M, 0.001 M KOH. All measurements were performed while stirring to prevent bubble formation. Region I (I_1, I_2, I_3) and II are marked and modes, were changes are visible, are highlighted. The depicted intensity from 700 to 1250 cm^{-1} is scaled by a factor of 10.

Upon increasing the electrode potential in 0.1 M KOH (Fig. 6a), the intensity of the peak I_3 and that of region II increase. Furthermore, the intensity of peak I_2 increases slightly compared to peak I_1. Additionally, the position of peak I_1 and I_3 shifts by approximately 6 cm^{-1} to 10 cm^{-1} upon increasing the electrode potential by 1.2 V (from 1.5 V). In region II, the changes observed are more complex, as region II separates into two bands, of which the band with the higher wavenumber also shifts by around 10 cm^{-1}. A shift of the band with a lower wavenumber of region II is not clearly visible, but its general shape changes with increasing potential. A similar effect is observed in measurements using electrolytes with varying pH, such as 0.1 M, 0.01 M, 0.001 M KOH while applying a potential of 1.64 V (Fig. 6b). Note that, as shown above, when the ionic concentration is kept constant, the Raman peaks do not shift when varying the pH (compare the black and orange curves in Fig. 2 for NiOOH).

The ionic strength influences local interfacial electric fields at the surface, similar to the applied potential, which in turn perturbs vibrational modes and is manifested by a vibrational Stark effect.[103] Such Stark effects have previously been observed in SERS studies of adsorbed species such as CO on Pd or Pt, affecting both the position (by up to 5.3 cm^{-1} per 0.1 V step) and the intensity of the vibrational modes.[104–106]

Notably, the Stark effect alone accounts for all changes observed in both the fundamental modes and, hence, also for the changes observed in the overtone regions II and III. Consequently, possible structural modifications or the presence of adsorbed species as well as associated OER mechanism that were attributed based on changes in this region might have to be reconsidered.[32,51,70]

Surface structure of NiOOH

Our combined Raman and DFT study shows that, after the electrochemical oxidation of $Ni(OH)_2$ (oxidation state 2.0), NiO_2 (oxidation state 4.0) is formed instead of the widely accepted NiOOH (oxidation state 3.0). Considering that previous studies report oxidation states for NiOOH ranging from 3.0 to 3.7,[32,36,43,107–109] it is very likely that Ni(IV) species must be present in the material with oxidation states larger than 3.0. The question thus arises whether these structures are completely mixed or differ at the electrode surface, near-surface region, and the bulk.

Bulk-sensitive EXAFS measurements in previous studies have revealed a Jahn–Teller

distortion in oxidized Ni samples, consistent with theoretical predictions for NiOOH.[39,49,109–111] In contrast, other EXAFS investigations on NiOOH films including $\gamma-$NiOOH with oxidation states exceeding 3.6 reported no evidence of a Jahn–Teller distortion.[32,49,112,113] Evidence for hydrogen in the bulk of NiOOH is substantiated by inelastic neutron scattering[42] and infrared spectroscopic experiments,[41,74,75] revealing hydrogen-bonded hydroxyl groups within the lattice.

Based on these findings, we infer that SER spectra mainly provide insights into the near-surface region, which appears to be oxidized to NiO_2, while the bulk could still remain as NiOOH. The high oxidation states of $\gamma-$NiOOH, which have been observed to range from 3.3 to 3.7, could be accounted for by a large surface area resulting from significant structural disorder, which is characteristic for $\gamma-$NiOOH.[36,107,114]

Conclusion

In this work, we investigated the oxidation of Ni in various alkaline electrolytes at potentials near and after the onset of the OER using SER spectroscopy. Furthermore, the underlying surface structure was elucidated by combining experiments in isotope-labeled water with DFT-computed Raman spectra. These combined findings illustrate that the surface primarily consists of $Ni(IV)O_2$ rather than the widely discussed Ni(III)OOH. Furthermore, we showed that the surface structure of $NiOOH/NiO_2$ in an alkaline environment is not directly affected by pH and cations such as Li^+ and K^+. Next, we attribute the experimentally observed Raman bands of $NiOOH/NiO_2$ between $900\,cm^{-1}$ and $1200\,cm^{-1}$, previously assigned to superoxides, to overtones and combination band. This assignment is further substantiated by the detection of second-order overtones in the SER spectra of $NiOOH/NiO_2$, as well as both first- and second-order overtones in the SER spectra of $Ni(OH)_2$. We propose that layered materials are particularly prone to exhibiting overtones, which should stimulate further fundamental Raman studies on this class of materials. Moreover, we rationalized the changes observed in the SER spectra in the overtone region at increasing potentials or ionic strength, previously assigned to structural changes of the material, to a vibrational Stark effect.

We believe that these findings are relevant for the ongoing discussion of the structure and understanding of the catalytic behavior of oxidized Ni anodes, in particular for the reaction mechanism of the OER. Moreover, they demonstrate that overtones can be observed in SER spectra, underscoring the importance of accounting for anharmonic effects in spectral analysis to avoid misinterpretation during material characterization

CRediT

J. Leist: Conceptualization, Formal Analysis, Investigation, Validation, Visualization, Writing - Original Draft Preparation. **A. Neufischer**: Investigation, Validation, Writing - Review & Editing. **T. Jacob**: Funding Acquisition, Resources, Supervision, Writing - Review & Editing. **A. K. Engstfeld**: Funding Acquisition, Conceptualization, Supervision, Writing - Review & Editing

Data Availability Statement

The data supporting the findings of this study are openly available in Zenodo at https://doi.org/10.5281/zenodo.17305627.

Acknowledgements

The authors gratefully acknowledge support from the DFG (German research foundation) through the collaborative research center CRC1316 (project 327886311) and the support by the state of Baden-Württemberg through bwHPC and the DFG through grant no INST 40/575-1 FUGG (JUSTUS 2 cluster).

Conflict of Interest

The authors declare no conflict of interest.

References

(1) Campion, A.; Kambhampati, P. Surface-Enhanced Raman Scattering. *Chemical Society Reviews* **1998**, *27*, 241–250.

(2) Han, X. X.; Rodriguez, R. S.; Haynes, C. L.; Ozaki, Y.; Zhao, B. Surface-Enhanced Raman Spectroscopy. *Nature Reviews Methods Primers* **2022**, *1*, 87.

(3) Smith, E.; Dent, G. *Modern Raman Spectroscopy – A Practical Approach*; John Wiley & Sons, Ltd, 2004.

(4) Moore, B. D.; Stevenson, L.; Watt, A.; Flitsch, S.; Turner, N. J.; Cassidy, C.; Graham, D. Rapid and Ultra-Sensitive Determination of Enzyme Activities Using Surface-Enhanced Resonance Raman Scattering. *Nature Biotechnology* **2004**, *22*, 1133–1138.

(5) Yilmaz, M.; Babur, E.; Ozdemir, M.; Gieseking, R. L.; Dede, Y.; Tamer, U.; Schatz, G. C.; Facchetti, A.; Usta, H.; Demirel, G. Nanostructured Organic Semiconductor Films for Molecular Detection with Surface-Enhanced Raman Spectroscopy. *Nature Materials* **2017**, *16*, 918–924.

(6) Brosseau, C. L.; Colina, A.; Perales-Rondon, J. V.; Wilson, A. J.; Joshi, P. B.; Ren, B.; Wang, X. Electrochemical Surface-Enhanced Raman Spectroscopy. *Nature Reviews Methods Primers* **2023**, *3*, 79.

(7) Hess, C. New Advances in Using Raman Spectroscopy for the Characterization of Catalysts and Catalytic Reactions. *Chemical Society Reviews* **2021**, *50*, 3519–3564.

(8) Stefancu, A. et al. Impact of Surface Enhanced Raman Spectroscopy in Catalysis. *ACS Nano* **2024**, *18*, 29337–29379.

(9) Han, X.-B.; Kannari, K.; Ye, S. *In Situ* Surface-Enhanced Raman Spectroscopy in Li–O2 Battery Research. *Current Opinion in Electrochemistry* **2019**, *17*, 174–183.

(10) Itoh, T.; Procházka, M.; Dong, Z.-C.; Ji, W.; Yamamoto, Y. S.; Zhang, Y.; Ozaki, Y. Toward a New Era of SERS and TERS at the Nanometer Scale: From Fundamentals to Innovative Applications. *Chemical Reviews* **2023**, *123*, 1552–1634.

(11) Wang, X.; Huang, S.-C.; Hu, S.; Yan, S.; Ren, B. Fundamental Understanding and Applications of Plasmon-Enhanced Raman Spectroscopy. *Nature Reviews Physics* **2020**, *2*, 253–271.

(12) Ding, S.-Y.; Yi, J.; Li, J.-F.; Ren, B.; Wu, D.-Y.; Panneerselvam, R.; Tian, Z.-Q. Nanostructure-Based Plasmon-Enhanced Raman Spectroscopy for Surface Analysis of Materials. *Nature Reviews Materials* **2016**, *1*, 16021.

(13) Zhang, Y.-J.; Ze, H.; Fang, P.-P.; Huang, Y.-F.; Kudelski, A.; Fernández-Vidal, J.; Hardwick, L. J.; Lipkowski, J.; Tian, Z.-Q.; Li, J.-F. Shell-Isolated Nanoparticle-Enhanced Raman Spectroscopy. *Nature Reviews Methods Primers* **2023**, *3*, 36.

(14) Schilling, C.; Hofmann, A.; Hess, C.; Ganduglia-Pirovano, M. V. Raman Spectra of Polycrystalline CeO2: A Density Functional Theory Study. *The Journal of Physical Chemistry C* **2017**, *121*, 20834–20849.

(15) Ozaki, Y.; Wójcik, M. J.; Popp, J. *Molecular Spectroscopy: A Quantum Chemistry Approach*; John Wiley & Sons, Ltd, 2019.

(16) Long, D. A. *The Raman Effect: A Unified Treatment of the Theory of Raman Scattering by Molecules*, 1st ed.; John Wiley & Sons, Ltd, 2002.

(17) Goulet, P. J. G.; Pieczonka, N. P. W.; Aroca, R. F. Overtones and Combinations in Single-Molecule Surface-Enhanced Resonance Raman Scattering Spectra. *Analytical Chemistry* **2003**, *75*, 1918–1923.

(18) Rubim, J. C.; Aroca, R. F. The Observation of High Order Overtones and Combinations in the SERRS Spectra of a Perylene Dye Spin Coated onto Silver Island Films. *Physical Chemistry Chemical Physics* **2008**, *10*, 5412–5418.

(19) Rao, R.; Tishler, D.; Katoch, J.; Ishigami, M. Multiphonon Raman Scattering in Graphene. *Physical Review B* **2011**, *84*, 113406.

(20) Malard, L. M.; Pimenta, M. A.; Dresselhaus, G.; Dresselhaus, M. S. Raman Spectroscopy in Graphene. *Physics Reports* **2009**, *473*, 51–87.

(21) Kupčić, I. Triple-Resonant Two-Phonon Raman Scattering in Graphene. *Journal of Raman Spectroscopy* **2012**, *43*, 1–5.

(22) Placidi, M.; Dimitrievska, M.; Izquierdo-Roca, V.; Fontané, X.; Castellanos-Gomez, A.; Pérez-Tomás, A.; Mestres, N.; Espindola-Rodriguez, M.; López-Marino, S.; Neuschitzer, M.; Bermudez, V.; Yaremko, A.; Pérez-Rodríguez, A. Multiwavelength Excitation Raman Scattering Analysis of Bulk and Two-Dimensional MoS2: Vibrational Properties of Atomically Thin MoS2 Layers. *2D Materials* **2015**, *2*, 035006.

(23) Liu, H.-L.; Yang, T.; Tatsumi, Y.; Zhang, Y.; Dong, B.; Guo, H.; Zhang, Z.; Kumamoto, Y.; Li, M.-Y.; Li, L.-J.; Saito, R.; Kawata, S. Deep-Ultraviolet Raman Scattering Spectroscopy of Monolayer WS2. *Scientific Reports* **2018**, *8*, 11398.

(24) Lyons, M. E.; Brandon, M. P. The Oxygen Evolution Reaction on Passive Oxide Covered Transition Metal Electrodes in Aqueous Alkaline Solution. Part 1-Nickel. *International Journal of Electrochemical Science* **2008**, *3*, 1386–1424.

(25) McCrory, C. C. L.; Jung, S.; Peters, J. C.; Jaramillo, T. F. Benchmarking Heterogeneous Electrocatalysts for the Oxygen Evolution Reaction. *Journal of the American Chemical Society* **2013**, *135*, 16977–16987.

(26) Trotochaud, L.; Young, S. L.; Ranney, J. K.; Boettcher, S. W. Nickel–Iron Oxyhydroxide Oxygen-Evolution Electrocatalysts: The Role of Intentional and Incidental Iron Incorporation. *Journal of the American Chemical Society* **2014**, *136*, 6744–6753.

(27) Michael, J. D.; Demeter, E. L.; Illes, S. M.; Fan, Q.; Boes, J. R.; Kitchin, J. R. Alkaline Electrolyte and Fe Impurity Effects on the Performance and Active-Phase Structure of NiOOH Thin Films for OER Catalysis Applications. *The Journal of Physical Chemistry C* **2015**, *119*, 11475–11481.

(28) Salmanion, M.; Najafpour, M. M. Oxygen-Evolution Reaction Performance of Nickel (Hydr)Oxide in Alkaline Media: Iron and Nickel Impurities. *The Journal of Physical Chemistry C* **2023**, *127*, 18340–18349.

(29) Dionigi, F.; Strasser, P. NiFe-Based (Oxy)Hydroxide Catalysts for Oxygen Evolution Reaction in Non-Acidic Electrolytes. *Advanced Energy Materials* **2016**, *6*, 1600621.

(30) Diaz-Morales, O.; Ferrus-Suspedra, D.; M. Koper, M. T. The Importance of Nickel Oxyhydroxide Deprotonation on

Its Activity towards Electrochemical Water Oxidation. *Chemical Science* **2016**, *7*, 2639–2645.

(31) Cui, X.; Ding, Y.; Zhang, F.; Cao, X.; Guo, Y.; Sun, L.; Zhang, B. Reserved Charges in a Long-Lived NiOOH Phase Drive Catalytic Water Oxidation. *Nature Chemistry* **2025**, 1–8.

(32) Lee, S.; Chu, Y.-C.; Bai, L.; Chen, H. M.; Hu, X. Operando Identification of a Side-on Nickel Superoxide Intermediate and the Mechanism of Oxygen Evolution on Nickel Oxyhydroxide. *Chem Catalysis* **2023**, *3*, 100475.

(33) Lee, S.; Banjac, K.; Lingenfelder, M.; Hu, X. Oxygen Isotope Labeling Experiments Reveal Different Reaction Sites for the Oxygen Evolution Reaction on Nickel and Nickel Iron Oxides. *Angewandte Chemie* **2019**, *131*, 10401–10405.

(34) Wei, J.; Shao, Y.; Xu, J.; Yin, F.; Li, Z.; Qian, H.; Wei, Y.; Chang, L.; Han, Y.; Li, J.; Gan, L. Sequential Oxygen Evolution and Decoupled Water Splitting via Electrochemical Redox Reaction of Nickel Hydroxides. *Nature Communications* **2024**, *15*, 9012.

(35) Bode, H.; Dehmelt, K.; Witte, J. Zur Kenntnis Der Nickelhydroxidelektrode—I.Über Das Nickel (II)-Hydroxidhydrat. *Electrochimica Acta* **1966**, *11*, 1079–1087.

(36) Oliva, P.; Leonardi, J.; Laurent, J. F.; Delmas, C.; Braconnier, J. J.; Figlarz, M.; Fievet, F.; de Guibert, A. Review of the Structure and the Electrochemistry of Nickel Hydroxides and Oxy-Hydroxides. *Journal of Power Sources* **1982**, *8*, 229–255.

(37) Alsabet, M.; Grdeń, M.; Jerkiewicz, G. Electrochemical Growth of Surface Oxides on Nickel. Part 3: Formation of β-NiOOH in Relation to the Polarization Potential, Polarization Time, and Temperature. *Electrocatalysis* **2015**, *6*, 60–71.

(38) Martirez, J. M. P.; Carter, E. A. Effects of the Aqueous Environment on the Stability and Chemistry of β-NiOOH Surfaces. *Chemistry of Materials* **2018**, *30*, 5205–5219.

(39) Hu, Q.; Xue, Y.; Kang, J.; Scivetti, I.; Teobaldi, G.; Selloni, A.; Guo, L.; Liu, L.-M. Structure and Oxygen Evolution Activity of β-NiOOH: Where Are the Protons? *ACS Catalysis* **2022**, *12*, 295–304.

(40) Fidelsky, V.; Butera, V.; Zaffran, J.; Toroker, M. C. Three Fundamental Questions on One of Our Best Water Oxidation Catalysts: A Critical Perspective. *Theoretical Chemistry Accounts* **2016**, *135*, 162.

(41) Kamath, P. V.; Ganguly, S. Infrared Spectroscopic Studies of the Oxide-Hydroxides of Ni, Co and Mn. *Materials Letters* **1991**, *10*, 537–539.

(42) Bantignies, J. L.; Deabate, S.; Righi, A.; Rols, S.; Hermet, P.; Sauvajol, J. L.; Henn, F. New Insight into the Vibrational Behavior of Nickel Hydroxide and Oxyhydroxide Using Inelastic Neutron Scattering, Far/Mid-Infrared and Raman Spectroscopies. *The Journal of Physical Chemistry C* **2008**, *112*, 2193–2201.

(43) Glemser, O.; Einerhand, J. Die Struktur höherer Nickelhydroxyde. *Zeitschrift für anorganische Chemie* **1950**, *261*, 43–51.

(44) McEwen, R. S. Crystallographic Studies on Nickel Hydroxide and the Higher Nickel Oxides. *The Journal of Physical Chemistry* **1971**, *75*, 1782–1789.

(45) Kim, M.-S.; Kim, K.-B. A Study on the Phase Transformation of Electrochemically Precipitated Nickel Hydroxides Using an Electrochemical Quartz Crystal

Microbalance. *Journal of The Electrochemical Society* **1998**, *145*, 507.

(46) Oesten, R.; Wohlfahrt-Mehrens, M.; Ströbele, S.; Kasper, M.; Huggins, R. A. Structural Aspects of Undoped and Doped Nickel Hydroxides. *Ionics* **1996**, *2*, 293–301.

(47) Ahn, H. S.; Bard, A. J. Surface Interrogation Scanning Electrochemical Microscopy of Ni1–xFexOOH (0 < x < 0.27) Oxygen Evolving Catalyst: Kinetics of the "Fast" Iron Sites. *Journal of the American Chemical Society* **2016**, *138*, 313–318.

(48) Barnard, R.; Randell, C. F.; Tye, F. L. Studies Concerning Charged Nickel Hydroxide Electrodes I. Measurement of Reversible Potentials. *Journal of Applied Electrochemistry* **1980**, *10*, 109–125.

(49) Bediako, D. K.; Lassalle-Kaiser, B.; Surendranath, Y.; Yano, J.; Yachandra, V. K.; Nocera, D. G. Structure–Activity Correlations in a Nickel–Borate Oxygen Evolution Catalyst. *Journal of the American Chemical Society* **2012**, *134*, 6801–6809.

(50) Merrill, M.; Worsley, M.; Wittstock, A.; Biener, J.; Stadermann, M. Determination of the "NiOOH" Charge and Discharge Mechanisms at Ideal Activity. *Journal of Electroanalytical Chemistry* **2014**, *717–718*, 177–188.

(51) Diaz-Morales, O.; Calle-Vallejo, F.; de Munck, C.; Koper, M. T. M. Electrochemical Water Splitting by Gold: Evidence for an Oxide Decomposition Mechanism. *Chemical Science* **2013**, *4*, 2334–2343.

(52) Gómez Meier, H.; Vilche, J. R.; Arvia, A. J. The Influence of Temperature on the Current Peak Multiplicity Related to the Nickel Hydroxide Electrode. *Journal of Applied Electrochemistry* **1980**, *10*, 611–621.

(53) Zhou, M.; Myung, N.; Chen, X.; Rajeshwar, K. Electrochemical Deposition and Stripping of Copper, Nickel and Copper Nickel Alloy Thin Films at a Polycrystalline Gold Surface: A Combined Voltammetry-Coulometry-Electrochemical Quartz Crystal Microgravimetry Study. *Journal of Electroanalytical Chemistry* **1995**, *398*, 5–12.

(54) Radinger, H.; Connor, P.; Tengeler, S.; Stark, R. W.; Jaegermann, W.; Kaiser, B. Importance of Nickel Oxide Lattice Defects for Efficient Oxygen Evolution Reaction. *Chemistry of Materials* **2021**, *33*, 8259–8266.

(55) Louie, M. W.; Bell, A. T. An Investigation of Thin-Film Ni–Fe Oxide Catalysts for the Electrochemical Evolution of Oxygen. *Journal of the American Chemical Society* **2013**, *135*, 12329–12337.

(56) Bernard, M. C.; Cortes, R.; Keddam, M.; Takenouti, H.; Bernard, P.; Senyarich, S. Structural Defects and Electrochemical Reactivity of Beta-Ni(OH)2. *Journal of Power Sources* **1996**, *63*, 247–254.

(57) Hermet, P.; Gourrier, L.; Bantignies, J.-L.; Ravot, D.; Michel, T.; Deabate, S.; Boulet, P.; Henn, F. Dielectric, Magnetic, and Phonon Properties of Nickel Hydroxide. *Physical Review B* **2011**, *84*, 235211.

(58) Klaus, S.; Cai, Y.; Louie, M. W.; Trotochaud, L.; Bell, A. T. Effects of Fe Electrolyte Impurities on Ni(OH)2/NiOOH Structure and Oxygen Evolution Activity. *The Journal of Physical Chemistry C* **2015**, *119*, 7243–7254.

(59) Murli, C.; Sharma, S. M.; S. K. Kulshreshtha; Sikka, S. K. High-Pressure Behavior of Beta-Ni (OH)2-A Raman Scattering Study. *Physica B: Condensed Matter* **2001**, *307*, 111–116.

(60) Brooker, M. H.; Hancock, G.; Rice, B. C.; Shapter, J. Raman Frequency and Intensity Studies of Liquid H2O, H218O and D2O. *Journal of Raman Spectroscopy* **1989**, *20*, 683–694.

(61) Desilvestro, J.; Corrigan, D. A.; Weaver, M. J. Spectroelectrochemistry of Thin Nickel Hydroxide Films on Gold Using Surface-Enhanced Raman Spectroscopy. *The Journal of Physical Chemistry* **1986**, *90*, 6408–6411.

(62) Desilvestro, J.; Corrigan, D. A.; Weaver, M. J. Characterization of Redox States of Nickel Hydroxide Film Electrodes by In Situ Surface Raman Spectroscopy. *Journal of The Electrochemical Society* **1988**, *135*, 885–892.

(63) Yeo, B. S.; Bell, A. T. In Situ Raman Study of Nickel Oxide and Gold-Supported Nickel Oxide Catalysts for the Electrochemical Evolution of Oxygen. *The Journal of Physical Chemistry C* **2012**, *116*, 8394–8400.

(64) Garcia, A. C.; Touzalin, T.; Nieuwland, C.; Perini, N.; Koper, M. T. M. Enhancement of Oxygen Evolution Activity of Nickel Oxyhydroxide by Electrolyte Alkali Cations. *Angewandte Chemie International Edition* **2019**, *58*, 12999–13003.

(65) Mavrič, A.; Fanetti, M.; Lin, Y.; Valant, M.; Cui, C. Spectroelectrochemical Tracking of Nickel Hydroxide Reveals Its Irreversible Redox States upon Operation at High Current Density. *ACS Catalysis* **2020**, *10*, 9451–9457.

(66) Moreno Fernández, H.; Alkemper, A.; Wang, K.; Mempin, C. J.; Gallenbeger, J.; Hofmann, J. P. Kinetic Analysis of the Self-Discharge of the NiOOH OER Active Phase in KOH Electrolyte: Insights from in-Situ Raman and UV–Vis Reflectance Spectroscopies. *Journal of Catalysis* **2024**, *440*, 115823.

(67) Lee, S.; Bai, L.; Hu, X. Deciphering Iron-Dependent Activity in Oxygen Evolution Catalyzed by Nickel–Iron Layered Double Hydroxide. *Angewandte Chemie International Edition* **2020**, *59*, 8072–8077.

(68) Suzuki, A.; Yaita, K.; Verma, G.; Jerkiewicz, G.; Tryk, D. A.; Kuzume, A. In Situ Shell-Isolated Nanoparticle-Enhanced Raman Spectroscopy Study of Nickel Surface Oxides Reveals Previously Unseen Surface Chemical Dynamics. *ACS Electrochemistry* **2025**,

(69) Melendres, C. A.; Paden, W.; Tani, B.; Walczak, W. On the Structure of the Higher Oxide Forms of Nickel. *Journal of The Electrochemical Society* **1987**, *134*, 762.

(70) Trześniewski, B. J.; Diaz-Morales, O.; Vermaas, D. A.; Longo, A.; Bras, W.; Koper, M. T.; Smith, W. A. In Situ Observation of Active Oxygen Species in Fe-Containing Ni-Based Oxygen Evolution Catalysts: The Effect of pH on Electrochemical Activity. *Journal of the American Chemical Society* **2015**, *137*, 15112–15121.

(71) Zhang, M.; de Respinis, M.; Frei, H. Time-Resolved Observations of Water Oxidation Intermediates on a Cobalt Oxide Nanoparticle Catalyst. *Nature Chemistry* **2014**, *6*, 362–367.

(72) Long, D. A. Infrared and Raman Characteristic Group Frequencies. Tables and Charts George Socrates John Wiley and Sons, Ltd, Chichester, Third Edition, 2001. Price £135. *Journal of Raman Spectroscopy* **2004**, *35*, 905–905.

(73) Hahn, F.; Beden, B.; Croissant, M. J.; Lamy, C. In Situ Uv Visible Reflectance Spectroscopic Investigation of the Nickel Electrode-Alkaline Solution Interface. *Electrochimica Acta* **1986**, *31*, 335–342.

(74) Casas-Cabanas, M.; D. Radin, M.; Kim, J.; P. Grey, C.; der Ven, A. V.;

Rosa Palacín, M. The Nickel Battery Positive Electrode Revisited: Stability and Structure of the β-NiOOH Phase. *Journal of Materials Chemistry A* **2018**, *6*, 19256–19265.

(75) Kober, F. P. Infrared Spectroscopic Investigation of Charged Nickel Hydroxide Electrodes. *Journal of The Electrochemical Society* **1967**, *114*, 215.

(76) Pushkarev, V. V.; Kovalchuk, V. I.; d'Itri, J. L. Probing Defect Sites on the CeO2 Surface with Dioxygen. *The Journal of Physical Chemistry B* **2004**, *108*, 5341–5348.

(77) Huang, Y.-F.; Kooyman, P. J.; Koper, M. T. M. Intermediate Stages of Electrochemical Oxidation of Single-Crystalline Platinum Revealed by in Situ Raman Spectroscopy. *Nature Communications* **2016**, *7*, 12440.

(78) He, Z.-D.; Tesch, R.; Eslamibidgoli, M. J.; Eikerling, M. H.; Kowalski, P. M. Low-Spin State of Fe in Fe-doped NiOOH Electrocatalysts. *Nature Communications* **2023**, *14*, 3498.

(79) Javad Eslamibidgoli, M.; Groß, A.; Eikerling, M. Surface Configuration and Wettability of Nickel(Oxy)Hydroxides: A First-Principles Investigation. *Physical Chemistry Chemical Physics* **2017**, *19*, 22659–22669.

(80) Song, F.; Busch, M. M.; Lassalle-Kaiser, B.; Hsu, C.-S.; Petkucheva, E.; Bensimon, M.; Chen, H. M.; Corminboeuf, C.; Hu, X. An Unconventional Iron Nickel Catalyst for the Oxygen Evolution Reaction. *ACS Central Science* **2019**, *5*, 558–568.

(81) Li, L.-F.; Li, Y.-F.; Liu, Z.-P. Oxygen Evolution Activity on NiOOH Catalysts: Four-Coordinated Ni Cation as the Active Site and the Hydroperoxide Mechanism. *ACS Catalysis* **2020**, *10*, 2581–2590.

(82) Conesa, J. C. Electronic Structure of the (Undoped and Fe-Doped) NiOOH O2 Evolution Electrocatalyst. *The Journal of Physical Chemistry C* **2016**, *120*, 18999–19010.

(83) Li, Y.-F.; Selloni, A. Mosaic Texture and Double C-Axis Periodicity of β-NiOOH: Insights from First-Principles and Genetic Algorithm Calculations. *The Journal of Physical Chemistry Letters* **2014**, *5*, 3981–3985.

(84) Moreno Fernández, H.; Karbasizadeh, S.; Adabifiroozjaei, E.; Molina-Luna, L.; Hofmann, J. P.; Amirabbasi, M. DFT-Guided Operando Raman Characterization of Ni-Oxide-Based Phases Relevant to Electrochemical Systems. *The Journal of Physical Chemistry C* **2025**, *129*, 16465–16476.

(85) Kresse, G.; Furthmüller, J. Efficiency of Ab-Initio Total Energy Calculations for Metals and Semiconductors Using a Plane-Wave Basis Set. *Computational Materials Science* **1996**, *6*, 15–50.

(86) Kresse, G.; Furthmüller, J. Efficient Iterative Schemes for Ab Initio Total-Energy Calculations Using a Plane-Wave Basis Set. *Physical Review B* **1996**, *54*, 11169–11186.

(87) Blöchl, P. E. Projector Augmented-Wave Method. *Physical Review B* **1994**, *50*, 17953–17979.

(88) Perdew, J. P.; Burke, K.; Ernzerhof, M. Generalized Gradient Approximation Made Simple. *Physical Review Letters* **1996**, *77*, 3865–3868.

(89) Grimme, S.; Antony, J.; Ehrlich, S.; Krieg, H. A Consistent and Accurate Ab Initio Parametrization of Density Functional Dispersion Correction (DFT-D) for the 94 Elements H-Pu. *The Journal of Chemical Physics* **2010**, *132*, 154104.

(90) Bonu, V.; Das, A.; Sivadasan, A. K.; Tyagi, A. K.; Dhara, S. Invoking Forbidden Modes in SnO2 Nanoparticles Using Tip Enhanced Raman Spectroscopy. *Journal of Raman Spectroscopy* **2015**, *46*, 1037–1040.

(91) Shahil, K. M. F.; Hossain, M. Z.; Teweldebrhan, D.; Balandin, A. A. Crystal Symmetry Breaking in Few-Quintuple Bi2Te3 Films: Applications in Nanometrology of Topological Insulators. *Applied Physics Letters* **2010**, *96*, 153103.

(92) Norton, R. D.; Phan, H. T.; Gibbons, S. N.; Haes, A. J. Quantitative Surface-Enhanced Spectroscopy. *Annual Review of Physical Chemistry* **2022**, *73*, 141–162.

(93) Wiesner, M.; Roberts, R. H.; Lin, J.-F.; Akinwande, D.; Hesjedal, T.; Duffy, L. B.; Wang, S.; Song, Y.; Jenczyk, J.; Jurga, S.; Mroz, B. The Effect of Substrate and Surface Plasmons on Symmetry Breaking at the Substrate Interface of the Topological Insulator Bi2Te3. *Scientific Reports* **2019**, *9*, 6147.

(94) Zhang, K.; Bao, C.; Gu, Q.; Ren, X.; Zhang, H.; Deng, K.; Wu, Y.; Li, Y.; Feng, J.; Zhou, S. Raman Signatures of Inversion Symmetry Breaking and Structural Phase Transition in Type-II Weyl Semimetal MoTe2. *Nature Communications* **2016**, *7*, 13552.

(95) Rodriguez, A.; Velický, M.; Ráhová, J.; Zólyomi, V.; Koltai, J.; Kalbáč, M.; Frank, O. Activation of Raman Modes in Monolayer Transition Metal Dichalcogenides through Strong Interaction with Gold. *Physical Review B* **2022**, *105*, 195413.

(96) Sun, L.; Yan, J.; Zhan, D.; Liu, L.; Hu, H.; Li, H.; Tay, B. K.; Kuo, J.-L.; Huang, C.-C.; Hewak, D. W.; Lee, P. S.; Shen, Z. X. Spin-Orbit Splitting in Single-Layer ${\mathrm{MoS}}_{2}$ Revealed by Triply Resonant Raman Scattering. *Physical Review Letters* **2013**, *111*, 126801.

(97) Ma, B.; D. Rodriguez, R.; Ruban, A.; Pavlov, S.; Sheremet, E. The Correlation between Electrical Conductivity and Second-Order Raman Modes of Laser-Reduced Graphene Oxide. *Physical Chemistry Chemical Physics* **2019**, *21*, 10125–10134.

(98) Gross, T.; Hess, C. Raman Diagnostics of LiCoO2 Electrodes for Lithium-Ion Batteries. *Journal of Power Sources* **2014**, *256*, 220–225.

(99) Angermann, M.; Jakopic, G.; Prietl, C.; Griesser, T.; Reichmann, K.; Deluca, M. Highly Conductive RuO2 Thin Films from Novel Facile Aqueous Chemical Solution Deposition. *Journal of Sol-Gel Science and Technology* **2023**, *108*, 575–587.

(100) Petrović, Z.; Ristić, M.; Marciuš, M.; Sepiol, B.; Peterlik, H.; Ivanda, M.; Musić, S. Formation of RuO2 Nanoparticles by Thermal Decomposition of Ru(NO)(NO3)3. *Ceramics International* **2015**, *41*, 7811–7815.

(101) Browne, M. P.; Sofer, Z.; Pumera, M. Layered and Two Dimensional Metal Oxides for Electrochemical Energy Conversion. *Energy & Environmental Science* **2019**, *12*, 41–58.

(102) Xie, H.; Li, Z.; Cheng, L.; Haidry, A. A.; Tao, J.; Xu, Y.; Xu, K.; Ou, J. Z. Recent Advances in the Fabrication of 2D Metal Oxides. *iScience* **2022**, *25*.

(103) Bhattacharyya, D.; E. Videla, P.; Cattaneo, M.; S. Batista, V.; Lian, T.; P. Kubiak, C. Vibrational Stark Shift Spectroscopy of Catalysts under the Influence of Electric Fields at Electrode–Solution Interfaces. *Chemical Science* **2021**, *12*, 10131–10149.

(104) Zou, S.; Weaver, M. J. Potential-Dependent Metal-Adsorbate Stretching Frequencies for Carbon Monoxide on Transition-Metal Electrodes: Chemical Bonding versus Electrostatic Field Effects. *The Journal of Physical Chemistry* **1996**, *100*, 4237–4242.

(105) Shi, H.; Cai, Z.; Patrow, J.; Zhao, B.; Wang, Y.; Wang, Y.; Benderskii, A.; Dawlaty, J.; Cronin, S. B. Monitoring Local Electric Fields at Electrode Surfaces Using Surface Enhanced Raman Scattering-Based Stark-Shift Spectroscopy during Hydrogen Evolution Reactions. *ACS Applied Materials & Interfaces* **2018**, *10*, 33678–33683.

(106) Oklejas, V.; Sjostrom, C.; Harris, J. M. Surface-Enhanced Raman Scattering Based Vibrational Stark Effect as a Spatial Probe of Interfacial Electric Fields in the Diffuse Double Layer. *The Journal of Physical Chemistry B* **2003**, *107*, 7788–7794.

(107) Corrigan, D. A.; Knight, S. L. Electrochemical and Spectroscopic Evidence on the Participation of Quadrivalent Nickel in the Nickel Hydroxide Redox Reaction. *Journal of The Electrochemical Society* **1989**, *136*, 613.

(108) Morishita, M.; Ochiai, S.; Kakeya, T.; Ozaki, T.; Kawabe, Y.; Watada, M.; Tanase, S.; Sakai, T. Phase Transformation in the Charge-Discharge Process and the Structural Analysis by Synchrotron XAFS and XRD for Nickel Hydroxide Electrode. *Electrochemistry* **2008**, *76*, 802–807.

(109) Farley, N. R. S.; Gurman, S. J.; Hillman, A. R. Dynamic EXAFS Study of Discharging Nickel Hydroxide Electrode with Non-Integer Ni Valency. *Electrochimica Acta* **2001**, *46*, 3119–3127.

(110) Pandya, K. I.; Hoffman, R. W.; McBreen, J.; O'Grady, W. E. In Situ X-Ray Absorption Spectroscopic Studies of Nickel Oxide Electrodes. *Journal of The Electrochemical Society* **1990**, *137*, 383.

(111) Tkalych, A. J.; Zhuang, H. L.; Carter, E. A. A Density Functional + U Assessment of Oxygen Evolution Reaction Mechanisms on β-NiOOH. *ACS Catalysis* **2017**, *7*, 5329–5339.

(112) Friebel, D.; Louie, M. W.; Bajdich, M.; Sanwald, K. E.; Cai, Y.; Wise, A. M.; Cheng, M.-J.; Sokaras, D.; Weng, T.-C.; Alonso-Mori, R.; Davis, R. C.; Bargar, J. R.; Nørskov, J. K.; Nilsson, A.; Bell, A. T. Identification of Highly Active Fe Sites in (Ni,Fe)OOH for Electrocatalytic Water Splitting. *Journal of the American Chemical Society* **2015**, *137*, 1305–1313.

(113) Zhao, T.; Shen, X.; Wang, Y.; Hocking, R. K.; Li, Y.; Rong, C.; Dastafkan, K.; Su, Z.; Zhao, C. In Situ Reconstruction of V-Doped Ni2P Pre-Catalysts with Tunable Electronic Structures for Water Oxidation. *Advanced Functional Materials* **2021**, *31*, 2100614.

(114) Glemser, O.; Einerhand, J. Über höhere Nickelhydroxyde. *Zeitschrift für anorganische Chemie* **1950**, *261*, 26–42.

Supplementary Files

This is a list of supplementary files associated with this preprint. Click to download.

- 2025JULENiRamansupportinginformation.pdf